

Resistive Memory Based on the Spin-Density-Wave Transition of Antiferromagnetic Chromium

Hongyu Chen, Zexin Feng, Peixin Qin, Xiaorong Zhou, Han Yan, Xiaoning Wang, Ziang Meng,
Li Liu, and Zhiqi Liu*

School of Materials Science and Engineering, Beihang University, Beijing 100191, China



(Received 20 July 2022; revised 19 September 2022; accepted 29 September 2022; published 16 November 2022)

Spin density waves (SDWs) are antiferromagnetic ground states characterized by real-space spin modulation. When an electronic system undergoes a paramagnetic-SDW transition, the translational symmetry is spontaneously broken and energy gaps are developed near the Fermi level, which offers potential for constructing various SDW components. Here we report a prototype resistive memory device based on a prototypical SDW metal, antiferromagnetic chromium. Transport and magnetic measurements show that the paramagnetic-SDW transition, i.e., the SDW antiferromagnetism, can be effectively suppressed by the electric-field-generated piezoelectric strain in epitaxial Cr/0.7Pb(Mg_{1/3}Nb_{2/3})O₃–0.3PbTiO₃ (PMN-PT) heterostructures. This enables a large electroresistance effect for metallic systems as the SDW band gaps can be intentionally controlled to vanish or develop. Combining this electroresistance effect with the different remanent piezoelectric strain of PMN-PT after poling by electric-field pulses of opposite polarity, we obtain two nonvolatile resistance states differing by about 1.8% and stable against a magnetic field of 3 T at room temperature. Our work unveils the electric-field controllability of the SDW transitions in thin films and the consequent wide application prospects of SDW materials.

DOI: 10.1103/PhysRevApplied.18.054046

I. INTRODUCTION

In electronic systems with strong electron-electron interactions and nested Fermi surfaces, electrons and holes can pair up and condense into an antiferromagnetic ground state as temperature decreases. Such ground states, characterized by periodically modulated spin density, are termed spin density waves (SDWs) [1]. Over the past decades, the intriguing physics of SDW states, such as unique dynamics [2], intertwining with superconductivity [3], and abnormal transport and magnetic phenomena [4,5], have attracted surges of interest.

On the other hand, the application potential of SDW states has seldom drawn much attention. It seems that the attributes that are necessary for achieving multiple functionalities for SDW systems have remained undiscovered up to now despite the aforementioned fruitful findings. In contrast, the field of charge density waves (CDWs)—the non-spin-polarized counterparts of SDWs—has undergone a rebirth recently, thanks to the layered van der Waals CDW crystals [6–10]. Thin films of these CDW materials have been exploited to construct numerous CDW devices that are regarded as contenders for future electronics.

It is interesting to notice that many of these CDW components are in fact designed based on a characteristic that is also shared by SDW materials—the stimuli-sensitive density-wave transitions [6–9]. Such transitions are always concomitant with changes in the electronic structure, and, more importantly, the transition process can be effectively tuned by proper external perturbations, such as strain, photons, and electric bias, which would result in prominent changes in physical responses. This offers significant potential for building functional devices. In this context, the paramagnetic-SDW (Néel) transitions with band-gap formation [11] can be a long-omitted merit of SDW materials, as they are expected to enable different functionalities as well. Moreover, the spontaneous coexistence of antiferromagnetism and density-wave ground states in SDW systems may lead to additional advantages and applications over the nonmagnetic CDW cases.

In this work, we employ a prototypical SDW metal, antiferromagnetic chromium [12], to unveil the application potential of SDW materials. Although Cr is a three-dimensional SDW system with partially gapped Fermi surfaces, we obtain several meaningful results that deserve detailed discussions and hold advantages for practical application. Bulk Cr spontaneously enters an incommensurate transverse SDW state below its Néel temperature (T_N) of approximately 311 K due to Fermi-surface nesting [13], where the SDW wave vectors align perpendicularly

* zhiqi@buaa.edu.cn

to the spins; at $T_{SF} \sim 123$ K, a spin-flip transition takes place and the transverse SDWs evolve to be longitudinal [12]. For thin films of Cr, the SDW order can be more complicated owing to strain and defects [14]. The T_{SF} can drastically vary and a commensurate SDW phase might develop and persist well above the bulk T_N . Additionally, the Néel transition is always broadened as the local T_N diverges in different areas. The SDW band gaps of Cr that lead to sudden increases of several percent (for bulk) or anomalies (for thin films) in resistivity, specific heat, etc. around T_N [12,14,15] have been experimentally verified [16,17]. Moreover, considerable efforts have been dedicated to tune the Néel transition of bulk Cr, and laborious methods such as hydrostatic pressure [18–20] and alloying [15,21] are necessary to produce notable effects owing to its three-dimensional metallic nature.

Based on these pioneering works, here we realize the electric-field modulation of the Néel transition of Cr via depositing its epitaxial thin films onto (001)-oriented ferroelectric $0.7\text{Pb}(\text{Mg}_{1/3}\text{Nb}_{2/3})\text{O}_3 - 0.3\text{PbTiO}_3$ (PMN-PT) substrates to construct multiferroic heterostructures [22–24]. Transport and magnetic measurements show that electric fields, mediated by the [110] compressive piezoelectric strain of PMN-PT, can suppress the formation of SDWs. The T_N deduced from the transport properties is decreased by around 9 K by an electric field of approximately -6.67 kV cm^{-1} , which results in a large electroresistance ratio (ER) for metallic systems of about 5.9% at 283 K. Furthermore, Cr/PMN-PT can exhibit two room-temperature nonvolatile resistance states that differ by around 1.8% and are stable against a magnetic field of 3 T after poling by different electric-field pulses. Our study not only demonstrates an energy-efficient prototype memory device based on a SDW metal, but also implies a feasible tactic to build various SDW components via tuning the SDW transitions and band gaps of thin films. For example, the electric-field-controllable SDW antiferromagnetism shown in our work can be exploited to build antiferromagnetic spintronic devices.

II. EXPERIMENTAL METHODS

A dc magnetron sputtering system is employed to fabricate Cr/PMN-PT heterostructures with a base pressure of around 7.5×10^{-9} Torr. The substrate temperature, sputtering power, Ar pressure, and distance between the target and substrates are kept at 450 °C, 30 W, 3 mTorr, and 245 mm during deposition, respectively. The deposition rate of Cr is approximately 0.22 \AA s^{-1} . The film thickness is approximately 80 nm unless otherwise noted. The samples are annealed at 450 °C *in situ* for 1 h after deposition and then cooled down to room temperature at a rate of about $2 \text{ }^\circ\text{C min}^{-1}$.

Temperature-dependent transport and magnetic properties are measured via a Quantum Design VersaLab system

with Keithley source meters to supply voltage or current and Keithley nanovoltmeters to measure voltage. The standard four-probe method is employed to determine the longitudinal resistivity while Hall bars are patterned to conduct the Hall measurement. All the temperature-dependent resistivity curves are measured in a warming-up procedure with a rate of approximately 1 K min^{-1} . A vibrating sample magnetometer module is employed to obtain magnetization loops. For the exchange-bias measurement, the thickness of $\text{Co}_{90}\text{Fe}_{10}$ (Co-Fe) is selected to be approximately 5 nm and the Pt/Co-Fe/Cr/PMN-PT stack is annealed at 400 K for 1 h with a magnetic field of 1.5 T applied along Cr⟨100⟩ to establish effective exchange bias.

In the transport measurements with *in situ* electric fields, a negative voltage of -200 V is applied across the heterostructure at room temperature before cooling it down in order to generate effective polarization switching. On the other hand, the voltage is applied at room temperature but turned off before testing the magnetic properties of the electric-field-poled samples. The electric fields within the 0.3-mm-thick PMN-PT substrate are calculated to be approximately -6.67 kV cm^{-1} .

A strain gauge is stuck onto a Pt(2 nm)/PMN-PT sample to measure the piezoelectric strain. Note that the measured values could be smaller than those exerted on Cr due to the loss of strain in the adhesive layer.

III. RESULTS AND DISCUSSION

A. Structural, magnetic, and transport properties

The PMN-PT substrates used in our study are at the morphotropic phase boundary [25,26]. The pseudocubic crystal structure of PMN-PT ($a \sim 4.02 \text{ \AA}$) [26] allows Cr to epitaxially grow on its (001) crystal planes with Cr⟨100⟩ parallel to PMN-PT ⟨110⟩ and the lattice mismatch is approximately -1.3% . The epitaxy of Cr/PMN-PT heterostructures is confirmed by x-ray diffraction (XRD). As shown in Fig. 1(a), the sharp (002) diffraction peak of the Cr thin film, together with the (002) and (003) peaks of PMN-PT in the XRD pattern, is in good accordance with the expected epitaxial relation. The linear dependence of the magnetic moment and Hall resistivity on applied fields in Figs. 1(b) and 1(c) is consistent with the antiferromagnetism of Cr. Additionally, the Hall data collected in our measurement geometry indicates that the transport properties are dominated by holes in Cr/PMN-PT. The deduced hole density nonmonotonically varies with temperature (T), which could result from the SDW nature of Cr (Note 1, Supplemental Material [27]). In addition, the absence of anomalous Hall-like signals also reveals a relatively low defect concentration [29].

Temperature-dependent longitudinal resistivity (ρ) is measured from 50 to 320 K. As depicted in Fig. 1(d), Cr/PMN-PT exhibits metallic transport behavior, i.e., its

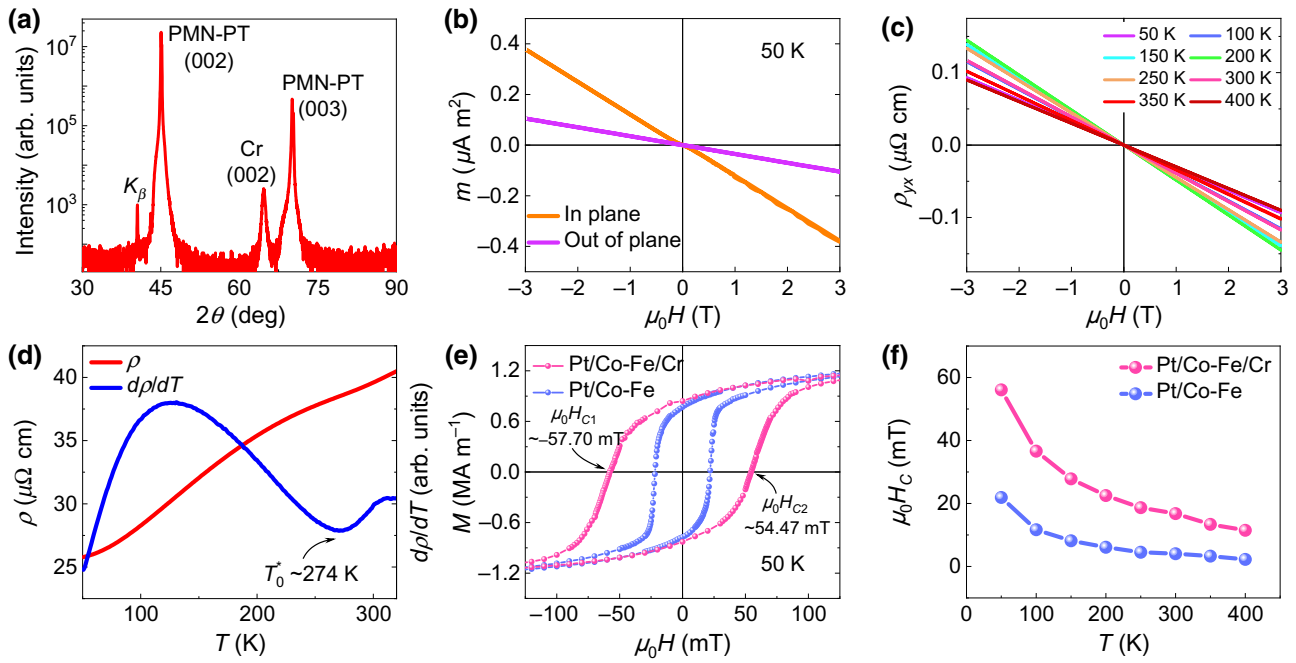


FIG. 1. Structural, magnetic, and transport properties of Cr/PMN-PT heterostructures. (a) X-ray diffraction pattern. Magnetic field ($\mu_0 H$)-dependent (b) magnetic moment (m) at 50 K and (c) Hall resistivity (ρ_{yx}) at various temperatures (T). (d) T -dependent resistivity (ρ) and the corresponding first derivative of ρ with respect to T ($d\rho/dT$). T_0^* denotes the T where $d\rho/dT$ reaches a minimum. (e) Magnetization (M) loops of Pt/Co-Fe/Cr/PMN-PT and Co-Fe/PMN-PT at 50 K. $\mu_0 H_{C1}$ and $\mu_0 H_{C2}$ represent the coercivity field of Pt/Co-Fe/Cr/PMN-PT. (f) $\mu_0 H_C$ of Pt/Co-Fe/Cr/PMN-PT and Co-Fe/PMN-PT as a function of T .

ρ increases with increasing T . The room-temperature resistivity is approximately $39.6 \mu\Omega \text{ cm}$, comparable to that of bulk and single-crystal thin films [5,30–32]. In addition, the first derivative of ρ with respect to T ($d\rho/dT$) is taken to monitor the phase-change process. As shown in Fig. 1(d), an anomaly shows up as a minimum [$(d\rho/dT)_{\min}$] at approximately 274 K. Generally, the temperature (denoted as T^* hereafter) where $(d\rho/dT)_{\min}$ emerges is recognized as the T_N of Cr [5,32,33]. However, the Néel transition of Cr thin films is in fact always broadened due to strain and defects [14] and a high- T_N commensurate SDW phase has been confirmed to survive well above T^* [33–36]. Accordingly, T^* cannot signify a critical point where the antiferromagnetic Cr uniformly converts to being paramagnetic, but it is reasonable to regard T^* as a temperature at which the Néel transition takes place most intensively.

Exchange bias [37] is an interfacial effect where the coupling of the interfacial moments of adjacent ferromagnetic and antiferromagnetic materials results in a biased magnetic hysteresis loop and enhanced coercivity (H_C). We then deposit Co-Fe and Pt layers onto a Cr/PMN-PT film at room temperature to confirm the antiferromagnetism of Cr below and above T^* . The exchange-bias field (H_{EB}) of the Pt/Co-Fe/Cr/PMN-PT stack is approximately -1.61 mT at 50 K [Fig. 1(e)]. It should be mentioned that H_{EB} is determined by complicated factors and the exchange-coupling energy deduced via H_{EB} has been

found to be relatively weak for Cr in general [37]. This is consistent with our results. Despite the small H_{EB} , the H_C of the sample is more than 2 times higher than that of a free Co-Fe layer [Fig. 1(e)]. At higher temperatures, although $|H_{EB}|$ decreases to zero at 275 K (Fig. S2, Supplemental Material [27]) owing to the intensive Néel transition, the H_C remains large even at 400 K [Fig. 1(f)], which is possibly due to the existence of the high- T_N commensurate SDW phase. Therefore, it is reasonable to infer that at least certain portions of the Cr/PMN-PT heterostructure retain antiferromagnetic SDW states above T^* .

B. Suppression of the Néel transition by electric fields

In order to clarify the effect of electric fields on the Néel transition, in Fig. 2 we compare the transport properties of Cr/PMN-PT with and without *in situ* electric fields. As shown in Fig. 2(c), an electric field of approximately -6.67 kV cm^{-1} obviously lowers the original T^* (denoted as T_0^* hereafter) from around 274 to 265 K (denoted as T_E^* hereafter), which indicates that electric fields can suppress the formation of the SDW phases. There are two main consequences of the suppressed Néel transition of Cr under electric fields that can offer potential for realizing different functionalities. The first one is weakened antiferromagnetism, which is evidenced by the decreased $|H_{EB}|$ of the Pt/Co-Fe/Cr/PMN-PT stack

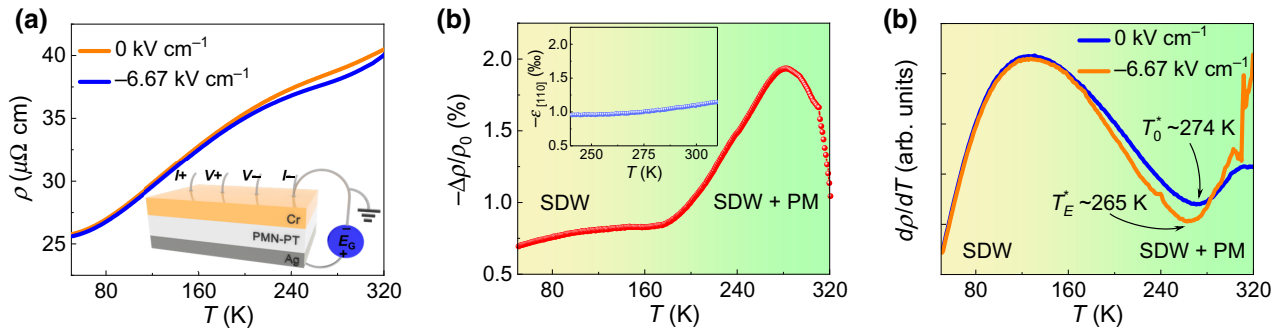


FIG. 2. Electric-field (E)-modulated transport properties. (a) $\rho(T)$ curves with and without E . The inset illustrates the measurement geometry. (b) T -dependent negative changing ratio of ρ ($-\Delta\rho/\rho_0$) after the application of E . With increased T , the Cr layer gradually changes from spin-density-wave (SDW) states to being paramagnetic (PM). The inset shows the negative [110] compressive piezoelectric strain ($-\varepsilon_{[110]}$) of PMN-PT in an electric field of approximately -6.67 kV cm^{-1} as a function of T . (c) $d\rho/dT(T)$ curves with and without E . T_0^* is lowered to T_E^* by E .

after electric-field poling (Note 2, Supplemental Material [27]). The other one, which is more important in our work, concerns the transport properties.

As shown in Fig. 2(a), the ρ of Cr/PMN-PT is lowered by the applied electric field within the measurement T range, and the decrease in ρ is pronounced from around 240 to 315 K. For clarity, we extract the T -dependent negative changing ratio of ρ ($-\Delta\rho/\rho_0$) induced by the electric fields in Fig. 2(b). The $-\Delta\rho/\rho_0(T)$ curve displays two regions with distinct variation behavior. Below approximately 170 K, $-\Delta\rho/\rho_0$ slowly increases from around 0.7% to 0.8% with augmented T ; with further raised T , $-\Delta\rho/\rho_0$ rises in a more rapid manner and peaks at approximately 283 K with a maximum value of about 1.9%. Although the initial slow increase of $-\Delta\rho/\rho_0$ could relate to the change of the physical properties of PMN-PT with T that slightly modifies the electron scattering in Cr, its subsequent sharp augmentation and maximization cannot simply be interpreted in terms of PMN-PT and the tuned electron scattering. As we demonstrate in the following, ρ is sensitive to the [110] in-plane piezoelectric strain ($\varepsilon_{[110]}$). Nevertheless, $\varepsilon_{[110]}$ remains almost constant from 240 to 290 K and keeps rising until at least 310 K [inset of Fig. 2(b)], which is inconsistent with the variation of $-\Delta\rho/\rho_0$.

On the other hand, the complicated variation tendency of $-\Delta\rho/\rho_0$ at high temperatures should directly result from the suppressed Néel transition of Cr. Given that the local T_N in Cr thin films strongly diverges, the applied electric field can always transform certain areas in the films from antiferromagnets to paramagnets and lead to vanished SDW band gaps. Therefore, the ρ of the sample is expected to significantly decrease as soon as the Néel transition starts, with $-\Delta\rho/\rho_0$ most notable near T_0^* or T_E^* where the Néel transition proceeds most intensively. This is fully consistent with the results in Fig. 2(b). In addition, the maximum of $-\Delta\rho/\rho_0$ emerges at approximately 283 K, slightly higher than T_0^* and T_E^* . This can

originate from the shrinkage of the transition window, i.e., not only can electric fields decrease T_0^* , but they can influence the transition process as well. The transport properties of Cr/PMN-PT with different film thicknesses are also in line with this scenario (Note 3, Supplemental Material [27]).

C. Suppression mechanisms

Generally, an electric field (E) across a ferroelectric heterostructure can bring about two effects on the film layer: lattice strain [38–45] and interfacial polarization charges (the field effect) [46,47]. Given that $-\Delta\rho/\rho_0$ is maximized at 283 K owing to the suppression of SDWs, in Fig. 3(a) we measure the ρ - E relations at the same temperature to reveal the modulation mechanisms of E . Note that the maximum E of $\pm 6.67 \text{ kV cm}^{-1}$ in the scans exceeds the ferroelectric coercivity of PMN-PT, and the polarization switching is evidenced by the peaks of the leaky current in Fig. 3(b). The $\rho(E)$ curves maintain the same asymmetric butterflylike shape in three consecutive scan cycles, which is reminiscent of the piezoelectric strain- E loop of PMN-PT [Fig. 3(c)]. Based on these observations, the E -tuning scenario of electrostatic-carrier injection can be excluded. Firstly, such a mechanism is related to the dielectric properties of PMN-PT. Thus, it always leads to square $\rho(E)$ curves that are similar to dielectric polarization loops in shape [47]. Additionally, the carrier density of Cr deduced from the Hall measurement is of the order of 10^{22} cm^{-3} , corresponding to a Thomas-Fermi screening length of several angstroms [38], which is much smaller than the film thickness. Consequently, the effect of interfacial electrostatic charges on the ρ of Cr/PMN-PT is anticipated to be negligible and cannot lead to the large electroresistance in Fig. 3(a).

For bulk Cr, volume shrinkage owing to compressive strain can result in an intensive decrease in the area of

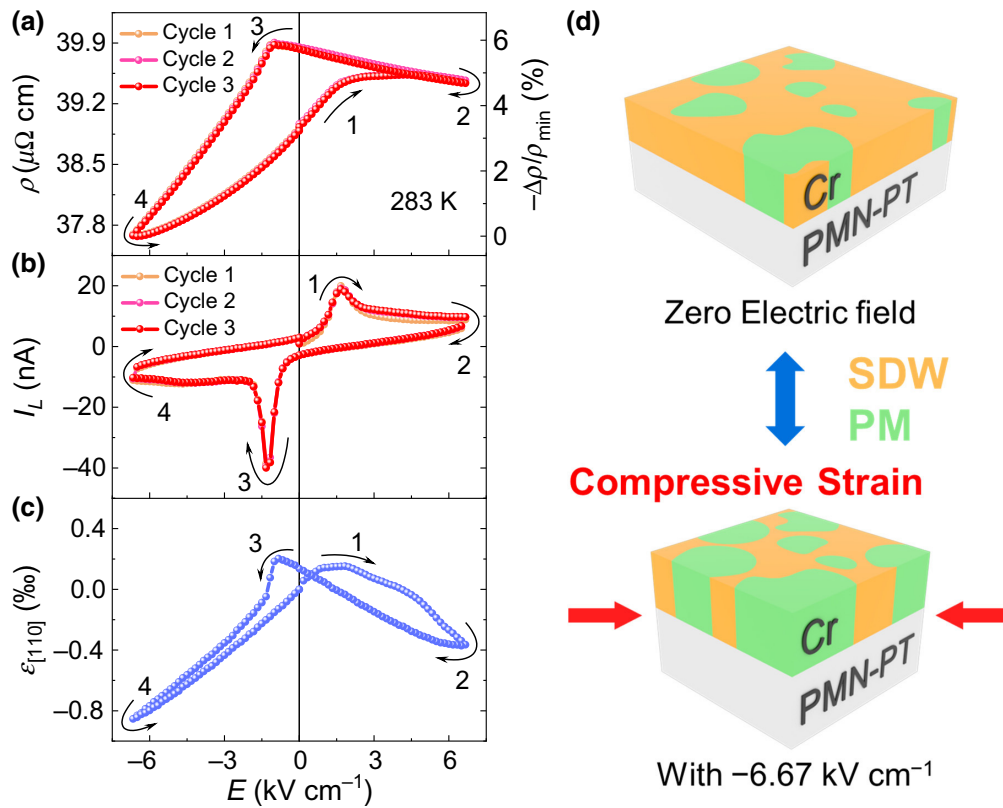


FIG. 3. Mechanisms of the E modulation. E -dependent (a) ρ of Cr/PMN-PT as well as the corresponding negative maximum ER ($-\Delta\rho/\rho_{\min}$), (b) leaky current (I_L), and (c) $\varepsilon_{[110]}$ of PMN-PT at 283 K. The curved arrows and numbers show the measurement procedure. (d) Schematics of the modulation mechanisms. The yellow and green regions represent the SDW antiferromagnetic and paramagnetic (PM) portions of the Cr layer, respectively.

certain portions of the Fermi surface that contribute to the nesting properties [19,21,48]. Thus, the stability of the SDWs is reduced and the T_N is lowered. For small strain, the T_N decreases linearly with pressure at a rate of approximately 5.1 K kbar^{-1} [18]. Furthermore, the T_N is more sensitive to longitudinal strain compared with shear strain, and the dependence is almost isotropic [49,50]. Accordingly, the effect of piezoelectric strain on the Néel transition of Cr can be interpreted as follows. The epitaxial Cr is nearly identically sensitive to in-plane strain along all directions. Owing to the larger piezoelectric strain along PMN-PT[110] than along PMN-PT[100] [51,52], the modulation effect is dominated by the former, leading to an asymmetric $\rho(E)$ curve that is similar to the $\varepsilon_{[110]}(E)$ curve of PMN-PT in shape [Fig. 3(c)], rather than the symmetric $\varepsilon_{[100]}-E$ relation [52]. Upon applying a negative E of approximately -6.67 kV cm^{-1} , a compressive piezoelectric strain of above -0.85% is exerted on Cr. Presuming that the elastic moduli of Cr thin films are of the same order of megabars as those of bulk [53], the T_N is anticipated to decrease by several kelvins according to the decreasing rate of approximately 5.1 K kbar^{-1} [18]. Consequently, certain portions of the antiferromagnetic Cr are

converted to be paramagnetic. This scenario is summarized in Fig. 3(d).

D. A large electroresistance effect for metallic systems

It is worth noting that the overall ER, i.e., the maximum negative changing ratio of ρ ($-\Delta\rho/\rho_{\min}$), reaches approximately 5.9% in Fig. 3(a), which is indeed large for general metallic systems. As discussed, the usual field effect is not expected to work in metals with carrier densities of $10^{22}\text{--}10^{23} \text{ cm}^{-3}$ due to electronic screening. Only when gated with a special polymeric electrolyte solution to induce a surface charge density of the order of 10^{15} cm^{-2} can the room-temperature ρ of a metallic thin film be modulated by approximately 4.7% [54]. Additionally, even though one utilizes piezoelectric strain rather than interfacial charges to tune transport properties, as in this work, the changes in ρ that result from the antiferromagnetic anisotropic magnetoresistance (AMR) effect and modified electron scattering due to lattice distortion remain far less than 1% in a normal alloy [43].

Historically, the large electroresistance effect for a metal in all-solid heterostructures has only been achieved based

on two mechanisms in different materials: the AMR effect from the strain-tunable magnetic anisotropy of Co [55] and the strain-sensitive first-order metamagnetic phase transition of FeRh [38,45]. Nevertheless, ferromagnetic metals that are both susceptible to strain and gifted with a large AMR effect can be scarce, while metallic metamagnetic materials can be even rarer. Here our results indicate an additional route to realize a large ER comparable to that of Co or FeRh for metallic systems: tuning the Néel transition and the SDW band gaps of SDW metals via piezoelectric strain.

Specifically, for Cr/PMN-PT, the dynamical piezoelectric strain exerted on Cr in the E scans can lower the local T_N by varying degrees and destroy the SDW band gaps to varying extents, which is supposed to alter the ρ by up to several percent according to the ρ changes in the Néel transition of Cr [19,56]. As a result, the ER is significantly enhanced compared to the case of normal metals and alloys. We further confirm this strain-mediated electroresistance mechanism in the thickness-dependent measurements (Note 4, Supplemental Material [27]). It should be clarified that the ER of approximately 5.9% is slightly higher than that extracted from the $\rho(T)$ curves. This discrepancy can be derived from the tensile piezoelectric strain of PMN-PT in E scans [Fig. 3(c)] that partially compensates the compressive epitaxial strain and leads to an increase in ρ . Additionally, we emphasize that the electroresistance cannot be exclusively credited to the tuned SDW transition. Considering that SDWs themselves are sensitive to strain as well [12,14], other factors such as the AMR effect [56] and the variation of SDW wavelength [5] could make moderate contributions too.

E. A prototype resistive memory device

The large electroresistance effect in a metallic system can be utilized for different applications. Here we employ Cr/PMN-PT to demonstrate a prototype ferroelectric memory device. Ferroelectric memristive components possess outstanding advantages in energy saving and high speed for writing a bit. Compared with other ferroelectric memories with a similar structure but based on (oxide) semiconductors, i.e., a thick ferroelectric layer sandwiched between a metallic electrode and a semiconducting film, which in fact can be regarded as ferroelectric field-effect transistors (FeFETs) [57–59] or piezoelectric-strain-based transistors (PSTs) [60–63], the advantages of using metallic Cr as the functional layer lie in the enhanced tolerance against defects, lowered working impedance, and improved stability against magnetic fields.

As shown in Fig. 4(a), the maximum ER is still above 5% at 300 K, as the electroresistance mechanism remains effective at room temperature due to the broadened Néel

transition. Ferroelectrics have been found to crack in repeated E cycles due to the fragility of domain boundaries [64]. Therefore, a unipolar-scan measurement is performed to prevent cracking [41,43,45], as depicted in Fig. 4(b). Notably, two nonvolatile resistance states differing by approximately 1.8% are found at zero field due to the remanent piezoelectric strain of PMN-PT, which can also be obtained via exciting the sample with E pulses of approximately 2.83 and -6.67 kV cm^{-1} [Fig. 4(c)]. Such room-temperature output is already comparable with or even larger than that of certain PSTs based on correlated oxides [60,62,63]. Moreover, these resistance states remain stable and differentiable even in a magnetic field of 3 T owing to the antiferromagnetic and metallic nature of Cr [Fig. 4(d)], which is an exclusive advantage inaccessible to other large-ER metals such as Co [55] and FeRh [38,45]. Additionally, compared with other magnetic-field-resistant memories based on the antiferromagnetic AMR effect, our prototype device of Cr/PMN-PT shows better distinguishability (one order of magnitude larger) of different resistance states [65,66].

We also notice that the current output signal of Cr/PMN-PT can be considerably smaller compared with the most outstanding cases among the aforementioned FeFETs and PSTs [57,59,61], which may obstruct it from practical application. Nevertheless, in principle, there can be several strategies to alleviate this problem, i.e., enhance the ER. The main factor that limits the overall ER lies in the relatively “mild” Néel transition in our samples, as shown in Fig. 2(a). In order to intensify the transition, i.e., narrow the transition window, the crystallization quality of Cr should be further improved to induce a more uniform local T_N and thus a sharper phase change. Note that this is also advantageous for the scalability of our design, as the impact of the nonuniform piezoelectric strain in PMN-PT can be minimized in this way at the same time. In this context, one can, for example, utilize other fabrication methods such as molecular beam epitaxy to directly deposit high-quality films, optimize the annealing process to reduce defect concentrations, or insert a metallic buffer layer to provide better conditions for crystallization. Moreover, via moderate alloying, the intrinsic changes in ρ in the SDW transition of Cr could also be enlarged [15]. On the other hand, the major factor that restricts the nonvolatile ER can lie in the relatively small [110] in-plane remanent piezoelectric strain of (001)-oriented PMN-PT. Therefore, one can employ other ferroelectric substrates with better piezoelectric properties, such as (011)-oriented PMN-PT [67], to improve the distinguishability. In addition, the limited T range for usage could be another shortcoming of our prototype device. Although we cannot completely circumvent this issue, we emphasize that the usage T of our design may be intentionally altered since the T_N of Cr is rather sensitive to alloying [15].

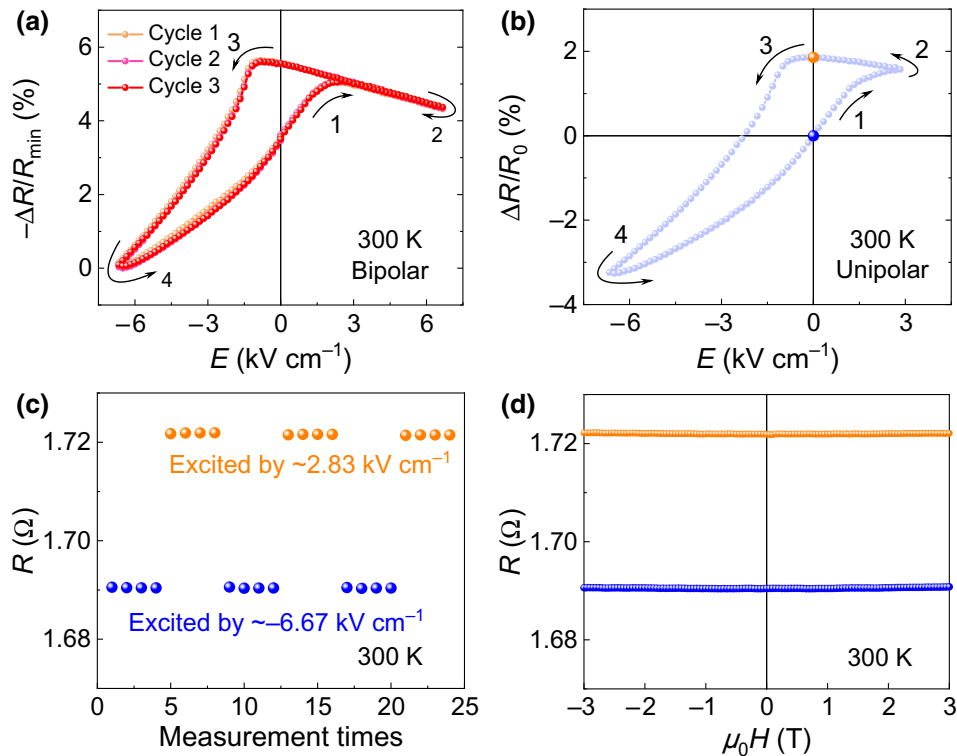


FIG. 4. A prototype resistive memory device at room temperature. (a) Negative maximum ER ($-\Delta R/R_{\min}$) in bipolar E scans and (b) ER ($\Delta R/R_0$) in unipolar E scans of Cr/PMN-PT. The curved arrows and numbers show the measurement procedure. (c) Binary memory functionality of Cr/PMN-PT with two nonvolatile resistance (R) states obtained after the excitation by E pulses of opposite polarity. (d) Magnetoresistance of the nonvolatile R states.

IV. CONCLUSION

In summary, we realize the E modulation of the Néel transition of Cr/PMN-PT heterostructures. It is discovered that the compressive piezoelectric strain generated by electric fields in Cr/PMN-PT can effectively suppress the formation of the SDW phase, which enables a large ER for metallic systems. Based on these findings, we demonstrate a room-temperature prototype binary resistive memory device that is stable against a magnetic field of 3 T. Our design could also be applied to SDW materials of lower dimensionality, where the Néel transition can induce more prominent changes in ρ , to achieve larger output signals.

In addition, we emphasize that our prototype device only exploits one of the results of tuning a paramagnetic-SDW transition. In recent years, antiferromagnetic spintronics has received extensive attention since antiferromagnets are considered as candidate materials for realizing ultrafast, field-resistant, and high-density electronics [68–72]. The efficient control of antiferromagnetism has been a core pursue of this field. Here we also demonstrate a tunable SDW antiferromagnetic order. Our method of manipulating antiferromagnetism via E holds prominent advantages of energy efficiency over other tactics such as current-induced torques [22]. The energy consumption of writing a bit is anticipated to be of the order of femtojoules or

even attojoules. Moreover, compared with other strategies based on E , such as the field effect, ionic-liquid gating, and electrochemical ionic migration, utilizing piezoelectric strain is unique in its nonvolatility owing to available different remanent-strain states, high speed due to the fast dynamics of ferroelectrics, and broad applicability as strain can effectively impact on both metals and oxides in a long-range manner [24]. Therefore, our work also indicates the potential of SDW materials for antiferromagnetic spintronic devices.

ACKNOWLEDGMENTS

Z.L. acknowledges financial support from the National Natural Science Foundation of China (Grants No. 52271235 and No. 52121001).

- [1] A. W. Overhauser, Giant Spin Density Waves, *Phys. Rev. Lett.* **4**, 462 (1960).
- [2] G. Grüner, The dynamics of spin-density waves, *Rev. Mod. Phys.* **66**, 1 (1994).
- [3] P. Dai, J. Hu, and E. Dagotto, Magnetism and its microscopic origin in iron-based high-temperature superconductors, *Nat. Phys.* **8**, 709 (2012).

- [4] F. Y. Yang and C. L. Chien, Oscillatory Exchange Bias due to an Antiferromagnet with Incommensurate Spin-Density Waves, *Phys. Rev. Lett.* **90**, 147201 (2003).
- [5] R. K. Kummamuru and Y.-A. Soh, Electrical effects of spin density wave quantization and magnetic domain walls in chromium, *Nature* **452**, 859 (2008).
- [6] M. J. Hollander, Y. Liu, W.-J. Lu, L.-J. Li, Y.-P. Sun, J. A. Robinson, and S. Datta, Electrically driven reversible insulator–metal phase transition in 1T-TaS₂, *Nano Lett.* **15**, 1861 (2015).
- [7] M. Yoshida, R. Suzuki, Y. Zhang, M. Nakano, and Y. Iwasa, Memristive phase switching in two-dimensional 1T-TaS₂ crystals, *Sci. Adv.* **1**, e1500606 (2015).
- [8] Y. Yu, F. Yang, X. F. Lu, Y. J. Yan, Y.-H. Cho, L. Ma, X. Niu, S. Kim, Y.-W. Son, D. Feng, *et al.*, Gate-tunable phase transitions in thin flakes of 1T-TaS₂, *Nat. Nanotechnol.* **10**, 270 (2015).
- [9] G. Liu, B. Debnath, T. R. Pope, T. T. Salguero, R. K. Lake, and A. A. Balandin, A charge-density-wave oscillator based on an integrated tantalum disulfide–boron nitride–graphene device operating at room temperature, *Nat. Nanotechnol.* **11**, 845 (2016).
- [10] A. A. Balandin, S. V. Zaitsev-Zotov, and G. Grüner, Charge-density-wave quantum materials and devices—New developments and future prospects, *Appl. Phys. Lett.* **119**, 170401 (2021).
- [11] A. W. Overhauser, Spin density waves in an electron gas, *Phys. Rev.* **128**, 1437 (1962).
- [12] E. Fawcett, Spin-density-wave antiferromagnetism in chromium, *Rev. Mod. Phys.* **60**, 209 (1988).
- [13] W. M. Lomer, Electronic structure of chromium group metals, *Proc. Phys. Soc.* **80**, 489 (1962).
- [14] H. Zabel, Magnetism of chromium at surfaces, at interfaces and in thin films, *J. Phys.: Condens. Matter* **11**, 9303 (1999).
- [15] E. Fawcett, H. L. Alberts, V. Y. Galkin, D. R. Noakes, and J. V. Yakhmi, Spin-density-wave antiferromagnetism in chromium alloys, *Rev. Mod. Phys.* **66**, 25 (1994).
- [16] A. S. Barker, B. I. Halperin, and T. M. Rice, Antiferromagnetic Energy Gap in Chromium, *Phys. Rev. Lett.* **20**, 384 (1968).
- [17] J. Schäfer, E. Rotenberg, G. Meigs, S. D. Kevan, P. Blaha, and S. Hüfner, Direct Spectroscopic Observation of the Energy Gap Formation in the Spin Density Wave Phase Transition at the Cr(110) Surface, *Phys. Rev. Lett.* **83**, 2069 (1999).
- [18] T. Mitsui and C. T. Tomizuka, Effect of hydrostatic pressure on the Néel temperature in chromium, *Phys. Rev.* **137**, A564 (1965).
- [19] D. B. McWhan and T. M. Rice, Pressure Dependence of Itinerant Antiferromagnetism in Chromium, *Phys. Rev. Lett.* **19**, 846 (1967).
- [20] I. S. Williams and R. Street, The effect of tensile stress on the Néel temperature in chromium, *Philos. Mag. B* **43**, 955 (1981).
- [21] T. M. Rice, A. S. Barker, B. I. Halperin, and D. B. McWhan, Antiferromagnetism in chromium and its alloys, *J. Appl. Phys.* **40**, 1337 (1969).
- [22] Z. Feng, H. Yan, and Z. Liu, Electric-field control of magnetic order: From FeRh to topological antiferromagnetic spintronics, *Adv. Electron. Mater.* **5**, 1800466 (2019).
- [23] Z. Liu, Z. Feng, H. Yan, X. Wang, X. Zhou, P. Qin, H. Guo, R. Yu, and C. Jiang, Antiferromagnetic piezospintrronics, *Adv. Electron. Mater.* **5**, 1900176 (2019).
- [24] H. Yan, Z. Feng, P. Qin, X. Zhou, H. Guo, X. Wang, H. Chen, X. Zhang, H. Wu, C. Jiang, *et al.*, Electric-field-controlled antiferromagnetic spintronic devices, *Adv. Mater.* **32**, 1905603 (2020).
- [25] S.-E. Park and T. R. Shrout, Ultrahigh strain and piezoelectric behavior in relaxor based ferroelectric single crystals, *J. Appl. Phys.* **82**, 1804 (1997).
- [26] B. Noheda, D. E. Cox, G. Shirane, J. Gao, and Z. G. Ye, Phase diagram of the ferroelectric relaxor $(1-x)\text{PbMg}_{1/3}\text{Nb}_{2/3}\text{O}_3-x\text{PbTiO}_3$, *Phys. Rev. B* **66**, 054104 (2002).
- [27] See Supplemental Material at <http://link.aps.org/supplemental/10.1103/PhysRevApplied.18.054046> for additional data of transport and magnetic measurements and related discussions, which includes reference [28].
- [28] S. Foner, Hall effect in titanium, vanadium, chromium, and manganese, *Phys. Rev.* **107**, 1513 (1957).
- [29] H. Chen, Z. Feng, H. Yan, P. Qin, X. Zhou, H. Guo, X. Wang, H. Wu, X. Zhang, Z. Meng, *et al.*, Anomalous Hall effect in antiferromagnetic Cr thin films, *Phys. Rev. B* **104**, 064428 (2021).
- [30] M. J. Marcinkowski and H. A. Lipsitt, Electrical resistivity of chromium in the vicinity of the Néel temperature, *J. Appl. Phys.* **32**, 1238 (1961).
- [31] S. Arajs and G. R. Dunmyre, Electrical resistivity and transverse electrical magnetoresistivity of chromium, *J. Appl. Phys.* **36**, 3555 (1965).
- [32] J. Mattson, B. Brumitt, M. B. Brodsky, and J. B. Ketterson, Magnetotransport studies of epitaxial Cr thin films, *J. Appl. Phys.* **67**, 4889 (1990).
- [33] J. Meersschaut, J. Dekoster, S. Demuynck, S. Cottenier, B. Swinnen, and M. Rots, Spin-density-wave magnetism in layered chromium studied by perturbed-angular-correlation spectroscopy, *Phys. Rev. B* **57**, R5575 (1998).
- [34] P. Sonntag, P. Bödeker, A. Schreyer, H. Zabel, K. Hamacher, and H. Kaiser, Magnetic phase diagram for spin-density waves in thin epitaxial Cr(001) films, *J. Magn. Magn. Mater.* **183**, 5 (1998).
- [35] P. Bödeker, A. Schreyer, and H. Zabel, Spin-density waves and reorientation effects in thin epitaxial Cr films covered with ferromagnetic and paramagnetic layers, *Phys. Rev. B* **59**, 9408 (1999).
- [36] E. Kunnen, S. Mangin, V. V. Moshchalkov, Y. Bruynseraede, A. Vantomme, A. Hoser, and K. Temst, Influence of strain on the anti-ferromagnetic ordering in epitaxial Cr(001) films on MgO, *Thin Solid Films* **414**, 262 (2002).
- [37] J. Nogués and I. K. Schuller, Exchange bias, *J. Magn. Magn. Mater.* **192**, 203 (1999).
- [38] Z. Q. Liu, L. Li, Z. Gai, J. D. Clarkson, S. L. Hsu, A. T. Wong, L. S. Fan, M. W. Lin, C. M. Rouleau, T. Z. Ward, *et al.*, Full Electroresistance Modulation in a Mixed-Phase Metallic Alloy, *Phys. Rev. Lett.* **116**, 097203 (2016).
- [39] Z. Q. Liu, H. Chen, J. M. Wang, J. H. Liu, K. Wang, Z. X. Feng, H. Yan, X. R. Wang, C. B. Jiang, J. M. D. Coey, *et al.*, Electrical switching of the topological anomalous Hall effect in a non-collinear antiferromagnet above room temperature, *Nat. Electron.* **1**, 172 (2018).

- [40] X. Wang, Z. Feng, P. Qin, H. Yan, X. Zhou, H. Guo, Z. Leng, W. Chen, Q. Jia, Z. Hu, *et al.*, Integration of the noncollinear antiferromagnetic metal Mn₃Sn onto ferroelectric oxides for electric-field control, *Acta Mater.* **181**, 537 (2019).
- [41] H. Yan, Z. Feng, S. Shang, X. Wang, Z. Hu, J. Wang, Z. Zhu, H. Wang, Z. Chen, H. Hua, *et al.*, A piezoelectric, strain-controlled antiferromagnetic memory insensitive to magnetic fields, *Nat. Nanotechnol.* **14**, 131 (2019).
- [42] H. Guo, Z. Feng, H. Yan, J. Liu, J. Zhang, X. Zhou, P. Qin, J. Cai, Z. Zeng, X. Zhang, *et al.*, Giant piezospintronic effect in a noncollinear antiferromagnetic metal, *Adv. Mater.* **32**, 2002300 (2020).
- [43] P. Qin, Z. Feng, X. Zhou, H. Guo, J. Wang, H. Yan, X. Wang, H. Chen, X. Zhang, H. Wu, *et al.*, Anomalous Hall effect, robust negative magnetoresistance, and memory devices based on a noncollinear antiferromagnetic metal, *ACS Nano* **14**, 6242 (2020).
- [44] Z. Feng, P. Qin, Y. Yang, H. Yan, H. Guo, X. Wang, X. Zhou, Y. Han, J. Yi, D. Qi, *et al.*, A two-dimensional electron gas based on a 5s oxide with high room-temperature mobility and strain sensitivity, *Acta Mater.* **204**, 116516 (2021).
- [45] Y. Lee, Z. Q. Liu, J. T. Heron, J. D. Clarkson, J. Hong, C. Ko, M. D. Biegalski, U. Aschauer, S. L. Hsu, M. E. Nowakowski, *et al.*, Large resistivity modulation in mixed-phase metallic systems, *Nat. Commun.* **6**, 5959 (2015).
- [46] C. H. Ahn, J. M. Triscone, and J. Mannhart, Electric field effect in correlated oxide systems, *Nature* **424**, 1015 (2003).
- [47] Z. Feng, H. Yan, X. Wang, H. Guo, P. Qin, X. Zhou, Z. Chen, H. Wang, Z. Jiao, Z. Leng, *et al.*, Nonvolatile electric control of the anomalous Hall effect in an ultrathin magnetic metal, *Adv. Electron. Mater.* **6**, 1901084 (2020).
- [48] P. A. Fedders and P. C. Martin, Itinerant antiferromagnetism, *Phys. Rev.* **143**, 245 (1966).
- [49] M. B. Walker, Phenomenological theory of the spin-density-wave state of chromium, *Phys. Rev. B* **22**, 1338 (1980).
- [50] W. C. Muir, E. Fawcett, and J. M. Perz, Magnetoelastic Properties of Single-*S*, Single-*Q* Chromium, *Phys. Rev. Lett.* **59**, 335 (1987).
- [51] S. Zhang, Y. G. Zhao, P. S. Li, J. J. Yang, S. Rizwan, J. X. Zhang, J. Seidel, T. L. Qu, Y. J. Yang, Z. L. Luo, *et al.*, Electric-Field Control of Nonvolatile Magnetization in Co₄₀Fe₄₀B₂₀/Pb(Mg_{1/3}Nb_{2/3})_{0.7}Ti_{0.3}O₃ Structure at Room Temperature, *Phys. Rev. Lett.* **108**, 137203 (2012).
- [52] L. Yang, Y. Zhao, S. Zhang, P. Li, Y. Gao, Y. Yang, H. Huang, P. Miao, Y. Liu, A. Chen, *et al.*, Bipolar loop-like non-volatile strain in the (001)-oriented Pb(Mg_{1/3}Nb_{2/3})O₃-PbTiO₃ single crystals, *Sci. Rep.* **4**, 4591 (2014).
- [53] K. W. Katahara, M. Nimalendran, M. H. Manghnani, and E. S. Fisher, Elastic moduli of paramagnetic chromium and Ti-V-Cr alloys, *J. Phys. F: Met. Phys.* **9**, 2167 (1979).
- [54] D. Daghero, F. Paolucci, A. Sola, M. Tortello, G. A. Ummarino, M. Agosto, R. S. Gonnelli, J. R. Nair, and C. Gerbaldi, Large Conductance Modulation of Gold Thin Films by Huge Charge Injection via Electrochemical Gating, *Phys. Rev. Lett.* **108**, 066807 (2012).
- [55] S.-W. Yang, R.-C. Peng, T. Jiang, Y.-K. Liu, L. Feng, J.-J. Wang, L.-Q. Chen, X.-G. Li, and C.-W. Nan, Non-volatile 180° magnetization reversal by an electric field in multiferroic heterostructures, *Adv. Mater.* **26**, 7091 (2014).
- [56] W. B. Muir and J. O. Ström-Olsen, Electrical resistance of single-crystal single-domain chromium from 77 to 325°K, *Phys. Rev. B* **4**, 988 (1971).
- [57] S. Mathews, R. Ramesh, T. Venkatesan, and J. Benedetto, Ferroelectric field effect transistor based on epitaxial perovskite heterostructures, *Science* **276**, 238 (1997).
- [58] T. Zhao, S. B. Ogale, S. R. Shinde, R. Ramesh, R. Droopad, J. Yu, K. Eisenbeiser, and J. Misewich, Colossal magnetoresistive manganite-based ferroelectric field-effect transistor on Si, *Appl. Phys. Lett.* **84**, 750 (2004).
- [59] M. Xu, J.-M. Yan, T.-W. Chen, Z.-X. Xu, H. Wang, L. Guo, G.-Y. Gao, S.-Y. Yan, F.-F. Wang, J.-X. Zhang, *et al.*, Room-temperature reversible and nonvolatile tunability of electrical properties of Cr-doped In₂O₃ semiconductor thin films gated by ferroelectric single crystal and ionic liquid, *Adv. Electron. Mater.* **5**, 1900212 (2019).
- [60] M. Zheng, H. Ni, Y. Qi, W. Huang, J. Zeng, and J. Gao, Ferroelastic strain control of multiple nonvolatile resistance tuning in SrRuO₃/PMN-PT(111) multiferroic heterostructures, *Appl. Phys. Lett.* **110**, 182403 (2017).
- [61] P. Salev, J. del Valle, Y. Kalcheim, and I. K. Schuller, Giant nonvolatile resistive switching in a Mott oxide and ferroelectric hybrid, *Proc. Natl. Acad. Sci. U.S.A.* **116**, 8798 (2019).
- [62] J.-M. Yan, M. Xu, T.-W. Chen, M.-M. Yang, F. Liu, H. Wang, L. Guo, Z.-X. Xu, F.-Y. Fan, G.-Y. Gao, *et al.*, Manipulation of the Electronic Transport Properties of Charge-Transfer Oxide Thin Films of NdNiO₃ Using Static and Electric-Field-Controllable Dynamic Lattice Strain, *Phys. Rev. Appl.* **11**, 034037 (2019).
- [63] M. Zheng, P. Guan, Y. Qi, and L. Guo, Straintronic effect on electronic transport and metal-insulator transition in correlated metal films by electric field, *Appl. Phys. Lett.* **120**, 161603 (2022).
- [64] Z. Q. Liu, J. H. Liu, M. D. Biegalski, J. M. Hu, S. L. Shang, Y. Ji, J. M. Wang, S. L. Hsu, A. T. Wong, M. J. Cordill, *et al.*, Electrically reversible cracks in an intermetallic film controlled by an electric field, *Nat. Commun.* **9**, 41 (2018).
- [65] X. Martí, I. Fina, C. Frontera, J. Liu, P. Wadley, Q. He, R. J. Paull, J. D. Clarkson, J. Kudrnovský, I. Turek, *et al.*, Room-temperature antiferromagnetic memory resistor, *Nat. Mater.* **13**, 367 (2014).
- [66] P. Wadley, B. Howells, J. Železný, C. Andrews, V. Hills, R. P. Campion, V. Novák, K. Olejník, F. Maccherozzi, S. S. Dhesi, *et al.*, Electrical switching of an antiferromagnet, *Science* **351**, 587 (2016).
- [67] M. Liu, B. M. Howe, L. Grazulis, K. Mahalingam, T. Nan, N. X. Sun, and G. J. Brown, Voltage-impulse-induced non-volatile ferroelastic switching of ferromagnetic resonance for reconfigurable magnetoelectric microwave devices, *Adv. Mater.* **25**, 4886 (2013).
- [68] T. Jungwirth, X. Martí, P. Wadley, and J. Wunderlich, Antiferromagnetic spintronics, *Nat. Nanotechnol.* **11**, 231 (2016).

- [69] V. Baltz, A. Manchon, M. Tsoi, T. Moriyama, T. Ono, and Y. Tserkovnyak, Antiferromagnetic spintronics, *Rev. Mod. Phys.* **90**, 015005 (2018).
- [70] P.-X. Qin, H. Yan, X.-N. Wang, Z.-X. Feng, H.-X. Guo, X.-R. Zhou, H.-J. Wu, X. Zhang, Z.-G.-G. Leng, H.-Y. Chen, *et al.*, Noncollinear spintronics and electric-field control: A review, *Rare Met.* **39**, 95 (2020).
- [71] H. Chen, P. Qin, H. Yan, Z. Feng, X. Zhou, X. Wang, Z. Meng, L. Lui, and Z. Liu, Noncollinear antiferromagnetic spintronics, *Mater. Lab* **1**, 220032 (2022).
- [72] Z. Feng, X. Zhou, L. Šmejkal, L. Wu, Z. Zhu, H. Guo, R. González-Hernández, X. Wang, H. Yan, P. Qin, *et al.*, An anomalous Hall effect in altermagnetic ruthenium dioxide, *Nat. Electron.* in press (2022).